environmental microbiology

Environmental Microbiology (2022) **00**(00), 00–00 doi:10.1111/1462-2920.16043

Biochemical and structural characterization of the cyanophage-encoded phosphate-binding protein: implications for enhanced phosphate uptake of infected cyanobacteria

Fangxin Zhao,[1,2†,‡] Xingqin Lin,[3,4†,‡] Kun Cai,[5,6†,‡] YongLiang Jiang,[5,6] Tianchi Ni,[3] Yue Chen,[1] Jianrong Feng,[3] Shangyu Dang,[2,3,7] Cong-Zhao Zhou[5,6*] and Qinglu Zeng [1,2,3,4,8*]

[1]*Department of Ocean Science, The Hong Kong University of Science and Technology, Clear Water Bay, Hong Kong, China.*

[2]*Southern Marine Science and Engineering Guangdong Laboratory (Guangzhou), Guangzhou, China.*

[3]*Division of Life Science, The Hong Kong University of Science and Technology, Clear Water Bay, Hong Kong, China.*

[4]*Southern Marine Science and Engineering Guangdong Laboratory (Zhuhai), Zhuhai, China.*

[5]*Hefei National Laboratory for Physical Sciences at the Microscale, University of Science and Technology of China, Hefei, Anhui, 230027, China.*

[6]*School of Life Sciences, University of Science and Technology of China, Hefei, Anhui, 230027, China.*

[7]*Center of Systems Biology and Human Health, Hong Kong University of Science and Technology, Clear Water Bay, Hong Kong, China.*

[8]*HKUST Shenzhen-Hong Kong Collaborative Innovation Research Institute, Futian, Shenzhen, China.*

Summary

To acquire phosphorus, cyanobacteria use the typical bacterial ABC-type phosphate transporter, which is composed of a periplasmic high-affinity phosphate-binding protein PstS and a channel formed by two transmembrane proteins PstC and PstA. A putative *pstS* gene was identified in the genomes of cyanophages that infect the unicellular marine cyanobacteria *Prochlorococcus* and *Synechococcus*. However, it has not been determined whether the cyanophage PstS protein is functional during infection to enhance the phosphate uptake rate of host cells. Here we showed that the cyanophage P-SSM2 PstS protein was abundant in the infected *Prochlorococcus* NATL2A cells and the host phosphate uptake rate was enhanced after infection. This is consistent with our biochemical and structural analyses showing that the phage PstS protein is indeed a high-affinity phosphate-binding protein. We further modelled the complex structure of phage PstS with host PstCA and revealed three putative interfaces that may facilitate the formation of a chimeric ABC transporter. Our results provide insights into the molecular mechanism by which cyanophages enhance the phosphate uptake rate of cyanobacteria. Phosphate acquisition by infected bacteria can increase the phosphorus contents of released cellular debris and virus particles, which together constitute a significant proportion of the marine dissolved organic phosphorus pool.

Introduction

Microorganisms are primarily responsible for the transformation of different chemical forms of phosphorus (P) in the oceans, the availability of which controls marine primary productivity (Karl, 2014). The unicellular picocyanobacterium *Prochlorococcus* is the dominant phytoplankton in tropical and subtropical oligotrophic oceans (Partensky *et al*., 1999; Scanlan *et al*., 2009), where phosphate concentrations are in the nanomolar range and can limit primary production (Wu *et al*., 2000; Thingstad *et al*., 2005). *Prochlorococcus* has evolved several mechanisms to adapt to low-P environments, including substituting non-phosphorus lipids for phospholipids (Van Mooy *et al*., 2006; Van Mooy *et al*., 2009) and encoding transporters for phosphonate and phosphite (Feingersch *et al*., 2012; Martinez *et al*., 2012). To store phosphate, *Prochlorococcus* maintains an extracellular buffer of labile phosphate (Zubkov *et al*., 2015). A proton

Received 14 January, 2022; revised 7 May, 2022; accepted 8 May, 2022. *For correspondence. E-mail zcz@ustc.edu.cn; Tel. 86-551-63600406, fax 86-0551-3600406. E-mail zeng@ust.hk; Tel. 852-2358-8701, fax 852-3693-4766. †These authors contributed equally to this work. ‡Fangxin Zhao, Xingqin Lin and Kun Cai are co-first authors.

motive force is required for the import of phosphate across the outer membrane into the periplasm (Kamennaya *et al*., 2020). To import phosphate from the periplasm into the cytoplasm, *Prochlorococcus* cells use the high-affinity phosphate-specific transport system (Pst) and do not encode low-affinity phosphate transporters (Moore *et al*., 2005; Scanlan *et al*., 2009). The Pst system has been extensively studied in *Escherichia coli* (Lamarche *et al*., 2008). This ABC-type phosphate transporter comprises the periplasmic high-affinity phosphate-binding protein PstS, a channel formed by two transmembrane proteins PstC and PstA, and the intracellular homodimeric ATPase PstB (Lamarche *et al*., 2008; Hsieh and Wanner, 2010). In response to P limitation, the PhoR/PhoB two-component signal transduction system upregulates the transcription of phosphate-acquisition genes (Nagaya *et al*., 1994; Suzuki *et al*., 2004; Tetu *et al*., 2009). Consistent with the upregulation of phosphate-acquisition genes (Martiny *et al*., 2006; Reistetter *et al*., 2013), the *Prochlorococcus* strain MED4 was shown to increase its maximum uptake velocity of phosphate under P-limited conditions (Krumhardt *et al*., 2013). *Prochlorococcus* field populations in low-P environments also show higher phosphate uptake velocities than those in high-P environments (Lomas *et al*., 2014).

Putative phosphate-acquisition genes have been found in the genomes of viruses (cyanophages) that infect *Prochlorococcus* and its closely related sister group marine *Synechococcus* (Sullivan *et al*., 2005; Sullivan *et al*., 2010). As lytic double-stranded DNA viruses, cyanophages comprise three morphotypes (Sullivan *et al*., 2003; Sabehi *et al*., 2012): T4-like and TIM5-like cyanomyoviruses, T7-like cyanopodoviruses and cyanosiphoviruses. Among the 77 publically available cyanomyovirus genomes in the NCBI database (as of August 2019), 24 carry *pstS* and three carry *phoA*, a putative alkaline phosphatase gene. It was thought that cyanophages carry phosphate-acquisition genes because of their significant phosphorus demand due to a high nucleic acid to protein ratio (Jover *et al*., 2014). Indeed, metagenomic analysis revealed that the frequencies of P-acquisition genes in the genomes of wild cyanomyoviruses are negatively correlated with the phosphate concentrations of the marine habitats (Kelly *et al*., 2013), which was also found in *Prochlorococcus* genomes (Martiny *et al*., 2006; Martiny *et al*., 2009; Coleman and Chisholm, 2010).

Our previous study found that *pstS* and *phoA* genes of cyanophage S-SM1 were upregulated during infection under P-limited conditions, and their expression was controlled by the host's PhoR/PhoB system (Zeng and Chisholm, 2012). Using cyanophage P-SSM2 that contains *pstS* but not *phoA*, our transcriptomic analysis further showed that *pstS* and the adjacent gene *g247* (with unknown function) were the only two phage genes that were upregulated when *Prochlorococcus* NATL2A was infected under P-limited conditions (Lin *et al*., 2016). Furthermore, we discovered that under P-limited conditions the host *pstS* transcripts per cell decreased after infection, whereas the phage *pstS* transcripts were much more abundant than the host copies, resulting in more *pstS* transcripts (host and phage combined) in the infected cells (Lin *et al*., 2016). However, it remains unknown whether phage PstS proteins are synthesized during infection to increase the phosphate uptake rate of infected *Prochlorococcus* cells.

Here, we investigate how the cyanophage PstS protein is integrated into the phosphate acquisition system of the cyanobacterial host. Using cyanophage P-SSM2 and *Prochlorococcus* NATL2A that we have studied previously (Zeng and Chisholm, 2012; Lin *et al*., 2016), we compared the phosphate-binding affinities of both phage and host PstS proteins, and then measured the PstS protein abundances during infection. We also compared phosphate uptake rates of infected and uninfected *Prochlorococcus* cells. To elucidate the molecular mechanism by which the phage PstS protein binds phosphate, we solved the crystal structures of cyanophage PstS proteins. Furthermore, modelling of cyanophage PstS binding to cyanobacterial PstCA predicted several essential residues for forming a chimeric ABC transporter.

Experimental procedures

Expression and purification of recombinant PstS proteins

The *pstS* genes of *Prochlorococcus* NATL2A, cyanophage P-SSM2 and cyanophage Syn19 were amplified by PCR using primers listed in Supplementary Table 1. PCR products were cloned into the pET-22b vector, and then transformed into *Escherichia coli* BL21 (DE3) cells harbouring the pKY206 plasmid. *Escherichia coli* cells were grown in 1 L LB medium (10 g Bacto tryptone, 10 g NaCl and 5 g yeast extract per litre) with 50 μg ml^{-1} ampicillin and 5 μg ml^{-1} tetracycline at 37°C for 5 h until $OD_{600} = 0.8$. Recombinant proteins with a C-terminal hexahistidine tag were induced with 0.2 mM IPTG for 20 h at 16°C. *Escherichia coli* cells were harvested by centrifugation at 8000*g* for 10 min and re-suspended in the lysis buffer (20 mM Tris–HCl, 200 mM NaCl, 5% glycerol, 5 mM sodium phosphate, pH 7.5). After sonication for 30 min, the cultures were spun down at 12 000*g* for 30 min and the supernatants were loaded onto a His-Select Nickel Affinity gel (GE Healthcare). Recombinant PstS proteins were eluted with the elution buffer (500 mM imidazole, 20 mM Tris–HCl, 200 mM NaCl, 5% glycerol, 5 mM sodium phosphate, pH 7.5) and then further purified using HiLoad 16/60 Superdex 200 columns (GE Healthcare). For crystallization, PstS

proteins with bound phosphate substrates were purified using HiLoad 16/60 Superdex 200 columns pre-equilibrated with 20 mM Tris–HCl, 200 mM NaCl, 5% glycerol, 5 mM sodium phosphate, 14 mM β-mercaptoethanol, pH 7.5. For phosphate-binding affinity assays, PstS proteins without bound phosphate substrates were purified using columns pre-equilibrated with 20 mM Tris–HCl, 200 mM NaCl, 5% glycerol, pH 7.5.

Measurement of phosphate-binding affinity of recombinant PstS proteins

Prior to the measurement of phosphate-binding affinity, we removed the residual phosphate substrates from the purified PstS proteins by dialyzing in the Tris buffer (20 mM Tris–HCl, 200 mM NaCl, pH 7.5) at 4°C for 24 h using the Slide-A-Lyzer mini dialysis devices (20K MWCO, Thermo Fisher Scientific). After dialysis, protein concentrations were measured using the DC Protein Assay Kit (Bio-Rad) with bovine serum albumin as standards.

Equilibrium dialysis was performed to determine the dissociation constant (K_d) of the recombinant PstS proteins (Poole and Hancock, 1984). In each Slide-A-Lyzer mini dialysis unit (20K), 4 μg protein was placed in the top dialysis chamber, and Tris buffer containing trace amount of ^{32}P-labelled orthophosphoric acid (~1.2 pmol and ~1 μCi, PerkinElmer) and different concentrations of cold phosphate (NaH_2PO_4) was placed in the bottom dialysis buffer chamber. After shaking for 24 h at room temperature, 100 μl samples were taken from the dialysis chamber and the dialysis buffer chamber respectively. Radioactivity was measured by adding the samples into 4 ml liquid scintillation cocktail (Optiphase HiSafe 3, PerkinElmer) and counting with a liquid scintillation counter (Wallac Win Spectral 1414, PerkinElmer). The dissociation constant K_d was determined using the following equation (Michaelis *et al*., 2011; Viaene *et al*., 2013):

$$B = \frac{B_{max} \times [L]}{[L] + K_d}$$

where B is the binding coefficient, B_{max} is the maximum binding coefficient and L is the concentration of free phosphate. Non-linear regression fitting was performed using SigmaPlot v12.5 (Systat Software). In Fig. 1, replicate dissociation constants were measured using separate batches of recombinant PstS proteins.

Infection of Prochlorococcus *NATL2A by cyanophages*

Infection of *Prochlorococcus* NATL2A by cyanophage P-SSM2 under P-limited conditions was carried out as we described previously (Zeng and Chisholm, 2012; Lin *et al*., 2016). The axenic *Prochlorococcus* NATL2A culture

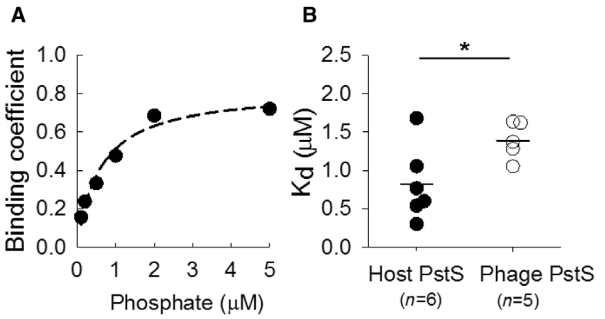

Fig. 1. Binding coefficient and dissociation constant of PstS proteins to phosphate.
A. A representative graph showing the binding coefficient of *Prochlorococcus* NATL2A PstS protein as a function of cold phosphate concentration. The binding coefficient is defined as the ratio of phosphate-bound PstS to the total PstS protein. A dashed line represents the non-linear regression curve fit to the Michaelis–Menten equation.
B. The dissociation constant K_d of the PstS protein to phosphate. Solid lines show the average PstS K_d values of *Prochlorococcus* NATL2A (host, $n = 6$) and cyanophage P-SSM2 (phage, $n = 5$) respectively. Asterisk indicates significant difference of K_d values of host and phage PstS proteins ($P = 0.038$, Student's *t*-test).

was maintained at 24°C under constant cool white light (~30 μE m^{-2} s^{-1}) in the Pro99 growth medium (Moore *et al*., 2002) that is based on Port Shelter seawater from Hong Kong. Fresh cyanophage P-SSM2 lysate was concentrated with Amicon Ultra-15 30K Centrifugal Filter Units (Millipore) at 3000*g* for 15 min, washed twice with sterile seawater, and re-suspended in the same medium. Prior to infection, mid-log *Prochlorococcus* NATL2A cultures were centrifuged at 10 000*g* for 15 min at 21°C, washed with the nutrient-replete Pro99 medium (with 50 μM phosphate) or the P-depleted Pro99 medium (without added phosphate), and re-suspended in the same media. After 24 h of re-suspension, *Prochlorococcus* NATL2A cells were mixed with cyanophage P-SSM2 at a phage/host ratio of 3. Following the same procedures, infection of *Prochlorococcus* NATL2A by cyanophage P-HM2 was carried out under P-limited conditions. Cell numbers were measured by flow cytometry (BD FACSCalibur, BD Biosciences). Extracellular P-SSM2 and P-HM2 phages were measured by quantitative PCR using primers for *g20* and *DNApol* respectively (Supplementary Table 1).

Quantification of host and phage PstS proteins using specific antibodies

The purified recombinant PstS proteins of *Prochlorococcus* NATL2A and cyanophage P-SSM2 were used as antigens to generate antibodies (Antibody host: rabbit; custom ordered from MW Biotech). The specificity of antibodies was confirmed using recombinant PstS proteins (Supplementary Fig. 1) and *Prochlorococcus* NATL2A cells (Fig. 2C).

To detect PstS proteins by Western blot, purified proteins or total proteins of *Prochlorococcus* cultures were denatured at 95°C for 15 min in the loading buffer (62.5 mM Tris-Cl, pH 6.8, 2% SDS, 0.05% bromophenol blue, 1% glycerol and 0.05% β-mercaptoethanol). Denatured proteins were separated on a 12% SDS-PAGE gel, stained with Coomassie Blue, and visualized with the ChemiDoc Imaging System (Bio-Rad). For Western blotting, proteins were transferred from the SDS-PAGE gel (without staining) onto a PVDF membrane and probed with primary antibodies against *Prochlorococcus* NATL2A PstS or cyanophage P-SSM2 PstS. The membrane was then incubated with an HRP-conjugated secondary antibody (ECL anti-rabbit IgG, GE Healthcare) and PstS bands were visualized with the ChemiDoc Imaging System (Bio-Rad).

For absolute quantification of PstS proteins in *Prochlorococcus* NATL2A cells, total proteins from 10^8 cells were separated on 12% SDS-PAGE alongside serial dilutions of purified recombinant PstS proteins with known amounts. Proteins were then transferred to a PVDF membrane for Western blot analysis using PstS antibodies (Fig. 2C). A standard curve was generated using the signal volume of recombinant PstS bands and the corresponding protein amounts (Supplementary Fig. 3A). Based on the standard curve, the average number of PstS protein molecules per cell was calculated (Supplementary Fig. 3B).

Phosphate uptake kinetics of Prochlorococcus *cells*

Phosphate uptake kinetics of *Prochlorococcus* NATL2A cells was measured following a method used previously for *Prochlorococcus* MED4 (Krumhardt *et al*., 2013), which

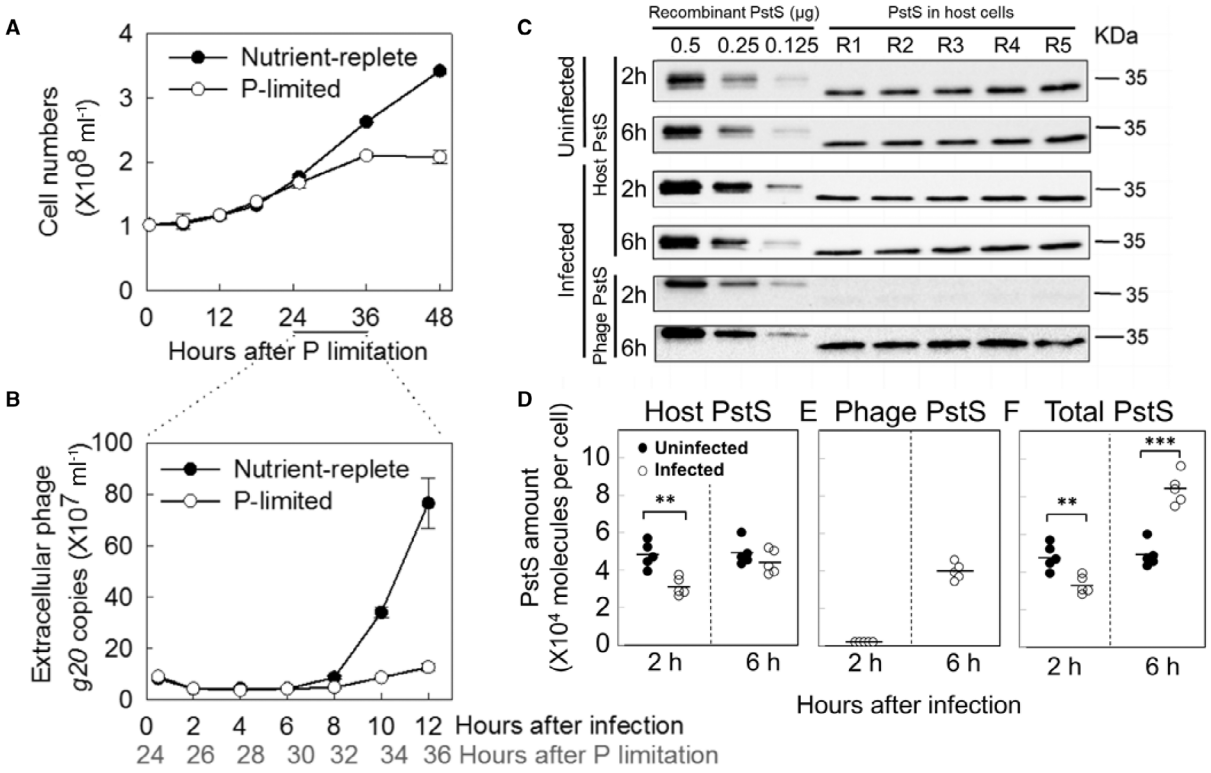

Fig. 2. Host and phage PstS protein abundances after *Prochlorococcus* NATL2A was infected by cyanophage P-SSM2.
A. *Prochlorococcus* NATL2A cells were spun down and re-suspended in nutrient-replete or P-limited growth media.
B. At 24 h after P limitation, *Prochlorococcus* NATL2A was infected by cyanophage P-SSM2 at a phage/host ratio of 3. Extracellular phages were measured by quantitative PCR using primers for the phage *g20* gene. Error bars in A and B indicate standard deviations from three biological replicates.
C. Quantitative Western blots of host and phage PstS proteins. At 2 and 6 h after infection under P-limited conditions, cells were collected by centrifugation, with five biological replicates for both uninfected and infected cultures (R1 to R5). Total proteins were separated on a 12% SDS-PAGE gel (10^8 cells per lane), transferred to a PVDF membrane, and probed with antibodies against host (top four panels) or phage PstS (bottom two panels). On the left of each gel, purified recombinant host (top four panels) or phage (bottom two panels) PstS proteins with known amounts (0.5, 0.25, 0.125 μg) were loaded as standards for protein quantification. Protein sizes are shown on the right.
D–F. At 2 and 6 h after infection under P-limited conditions, host (D), phage (E) and total (F) PstS proteins were quantified (Supplementary Fig. 3). Error bars indicate standard deviation of five biological replicates. Asterisks indicate significant changes in the infected cells compared to the uninfected cells (**P < 0.005 and ***P < 0.0001, Student's t-test).

takes about 2 h for each measurement. Briefly, 12 ml culture was centrifuged at 10 000*g* for 15 min at 21°C and re-suspended with the same volume of the Pro99 medium without addition of phosphate. After re-suspension, aliquots of 1 ml cultures were transferred to clear Eppendorf tubes, which contained trace amount of ^{32}P-labelled orthophosphoric acid (~1 μCi, Perkin Elmer) and different concentrations of cold PO_4 (0.02, 0.1, 0.2, 0.5, 1, 2.5, 5, 7.5, 10, 15 and 20 μM). Cultures were incubated for 60 min at 24°C at a light level of ~30 μE m^{-2} s^{-1} to allow linear uptake of phosphate (Supplementary Fig. 11). Cultures were then filtered at a vacuum pressure of ~100 mm Hg through a 0.22 μm polycarbonate filter that was supported by a Whatman GF/F filter. Prior to filtration, the filters were pre-soaked with the Pro99 medium amended with 0.5 mM PO_4 to minimize non-specific adhesion of ^{32}P on to the filters. After filtration, the filters were soaked in a basic oxalate reagent for 10 min and dried by filtration for 30 s. Since oxalate removes the extracellular phosphate buffer of cyanobacterial cells (Zubkov *et al*., 2015), the remaining ^{32}P reflected intracellular phosphate uptake by *Prochlorococcus* cells. The filters were immersed into 4 ml liquid scintillation cocktail (Optiphase HiSafe 3, Perkin Elmer) and the radioactivity of each filter was measured by a liquid scintillation counter (Wallac Win Spectral 1414, PerkinElmer). A filter without any cells was measured as a blank control to reflect the background ^{32}P level.

The phosphate uptake velocity (V) of *Prochlorococcus* NATL2A was determined by the following equation (Fu *et al*., 2005; Krumhardt *et al*., 2013):

$$V = [P(R_f - R_b)]/(R_t tcv)$$

where R_f is the ^{32}P radioactivity on the filters with cells, R_b denotes the radioactivity on the blank control filter without cells and R_t is the total radioactivity in the 1 ml culture. P is the concentration of cold PO_4 (amol per litre), while t, c and v represent incubation time (h), cell concentration (cells per litre) and volume of the filtered culture (litre) respectively. The velocity (amol $cell^{-1}$ h^{-1}) was plotted against cold phosphate concentration and the curve was fitted to the Michaelis–Menten equation:

$$V = (V_{max} \times P)/(K_M + P)$$

where V_{max} represents the maximum velocity of phosphate uptake and K_M represents the Michaelis–Menten constant. The non-linear regression was performed on SigmaPlotv12.5 (Systat Software, USA).

Crystallization of PstS with phosphate

Fractions containing the target protein were pooled and concentrated to 8 mg ml^{-1} for crystallization. Crystals were grown by mixing the protein sample with the reservoir solution at a 1:1 ratio in hanging drops at 13°C. The crystallization buffer was composed of 20 mM Tris–HCl, pH 7.5, 200 mM NaCl, 5% glycerol, 5 mM sodium phosphate buffer, pH 7.5, 1 mM DTT. Crystals of PstS from P-SSM2 appeared in the condition containing 25% (wt./vol.) polyethylene glycol 3350, 0.1 M citric acid, pH 3.5, while the Crystals of PstS from Syn19 appeared in the condition containing 18% (wt./vol.) polyethylene glycol 3350, 0.2 M sodium formate.

Data collection and structure determination

For diffraction analysis, the crystals were pooled and flash-frozen in liquid nitrogen after soaking in the glycerol cryoprotectant. X-ray diffraction data were collected at the beamline BL17U at the Shanghai Synchrotron Radiation Facility (SSRF). Diffraction images were processed and scaled with HKL-2000 program package (Otwinowski and Minor, 1997) to the highest resolutions of 2.25 Å for P-SSM2 PstS and 1.70 Å for Syn19 PstS respectively. The structures were determined by molecular replacement using the program Molrep of the CCP4 (Collaborative Computational Project, 1994) with *E. coli* PstS (PDB accession code 1IXH) as the search template (Wang *et al*., 1997). The structure refinement was performed by using the programs Coot (Emsley and Cowtan, 2004) and Refmac. The quality of the structures was analysed by MolProbity (Chen *et al*., 2010). The parameters of crystal data collection and structure refinement for P-SSM2 and Syn19 PstS proteins are listed in Supplementary Tables 2 and 3 respectively. All figures showing structures were prepared with PyMOL.

Modelling the interaction of cyanophage PstS with the host PstCA complex

We simulated the PstCA structure of *Prochlorococcus* NATL2A by SWISS-MODEL (https://swissmodel.expasy.org/) using the published structure of the maltose ABC transporter MalFG (Oldham *et al*., 2007). Then, we docked the phage PstS structure onto the simulated PstCA models using HADDOCK (https://alcazar.science.uu.nl/services/HADDOCK2.2/). HADDOCK clustered 103 structures in 11 clusters, which represent 51.5% of the water-refined models HADDOCK generated. The best cluster, which is the most reliable according to HADDOCK, possesses a Haddock score of −136.9 (±8.7), a Z-score of −2.2 and an RMSD value of 0.6 (±0.3) Å. The Z-score indicates how many standard deviations from the average this cluster is located in terms of score (the more negative the better).

Phylogenetic analysis

Among the 77 cyanomyovirus genomes available in the NCBI database (as of August 2019), PstS protein sequences were identified in 24 cyanomyovirus genomes. Those 24 cyanomyoviruses were shown to infect nine *Prochlorococcus* strains and four *Synechococcus* strains (Sullivan *et al*., 2003; Sullivan *et al*., 2010; Sabehi *et al*., 2012; Hua *et al*., 2017; Enav *et al*., 2018; Zborowsky and Lindell, 2019; Jiang *et al*., 2020; Wang *et al*., 2020). PstS protein sequences of the 24 cyanomyoviruses and 13 cyanobacterial host strains were downloaded from NCBI. For phylogenetic analysis, PstS protein sequences were aligned using Clustal Omega (Madeira *et al*., 2019) and visualized by BOXSHADE (https://embnet.vital-it.ch/software/BOX_form.html). Phylogenetic inference was based on the resulting alignment and conducted using the RAxML software (Stamatakis, 2014). The phylogenetic tree was visualized by Interactive Tree of Life (https://itol.embl.de/) (Letunic and Bork, 2016).

Results

Phosphate-binding affinities of Prochlorococcus *and cyanophage PstS proteins*

To compare the phosphate-binding affinities of PstS proteins encoded by *Prochlorococcus* NATL2A and cyanophage P-SSM2, we cloned their genes in *E. coli* and purified the recombinant PstS proteins (Supplementary Fig. 1A). The binding coefficient of PstS to phosphate (the ratio of phosphate-bound PstS to the total PstS protein) showed a typical hyperbolic relationship with phosphate concentration (Fig. 1A). The maximum binding coefficients (B_{max}) for host and phage PstS proteins were 0.71 $\pm$ 0.38 and 1.12 $\pm$ 0.14 respectively. This suggested that one PstS protein binds to one phosphate molecule, which is consistent with the stoichiometry of the *E. coli* PstS protein (B_{max} = 0.90) (Medveczky and Rosenberg, 1970; Luecke and Quiocho, 1990). The B_{max} values of PstS proteins could be affected by the ratios of different structural conformations, with the open conformation suitable for accepting phosphate while the close conformation inaccessible to phosphate (Brautigam *et al*., 2014). The dissociation constants (K_d) of the host and phage PstS proteins were 0.82 $\pm$ 0.44 and 1.39 $\pm$ 0.22 μM respectively, which are higher than those of *E. coli* (0.8 μM) and *Pseudomonas aeruginosa* (0.34 μM) (Medveczky and Rosenberg, 1970; Poole and Hancock, 1984).

Host and phage PstS protein abundances during infection under P-limited conditions

We used specific antibodies (Supplementary Fig. 1) to detect the host PstS protein in the uninfected cells. Similar to our previous studies (Zeng and Chisholm, 2012; Lin *et al*., 2016), from 24 h after resuspension in P-limited growth medium, *Prochlorococcus* NATL2A cells grew slower than those in the nutrient-replete medium (Fig. 2A). Both gel electrophoresis and Western blot analyses showed that the PstS protein abundance gradually increased during the progression of P limitation, while it was undetectable under nutrient-replete conditions (Supplementary Fig. 2). The results are consistent with the changes of PstS protein abundances in response to P limitation in *Prochlorococcus* MED4 (Fuszard *et al*., 2010), *Synechococcus* WH7803 (Scanlan *et al*., 1993) and *Synechococcus* WH8102 (Ostrowski *et al*., 2010; Cox and Saito, 2013).

To measure the abundances of host and phage PstS proteins, we infected *Prochlorococcus* NATL2A with cyanophage P-SSM2 (phage/host ratio = 3) at 24 h of P limitation when the host PstS protein had been highly induced (Supplementary Fig. 2). Consistent with previous studies (Zeng and Chisholm, 2012; Lin *et al*., 2016), progeny phages were released after 8 h of infection and fewer phages were produced under P-limited conditions than those under nutrient-replete conditions (Fig. 2B). Using quantitative Western blotting (Fig. 2C, Supplementary Fig. 3), we found that under P-limited conditions the uninfected cultures had an average of 48 480 $\pm$ 6393 PstS protein molecules per cell, which is comparable to that of *E. coli* (Medveczky and Rosenberg, 1970). During infection under P-limited conditions, the host PstS protein abundances decreased significantly by 35% at 2 h and decreased by 10% at 6 h, compared with those of uninfected cells at the same time points (Fig. 2D). The phage PstS protein was barely detected at 2 h after infection (Fig. 2C), but increased at 6 h to 81% of the host PstS abundance in the uninfected cultures (Fig. 2E). As a result of the high expression level of phage PstS proteins, the total PstS proteins were 71% more abundant than those in the uninfected cultures (Fig. 2F).

Phosphate uptake kinetics of Prochlorococcus *after phage infection*

Having shown that cyanophage-encoded PstS protein can bind phosphate and was expressed during infection, we wondered whether cyanophage infection affects the phosphate uptake kinetics of *Prochlorococcus* cells. We used an established ^{32}P tracer method (see Experimental procedures) that has been used to measure the intracellular phosphate uptake of *Prochlorococcus* MED4 (Krumhardt *et al*., 2013). The phosphate uptake velocity forms a hyperbolic relationship with phosphate concentration (Supplementary Fig. 4A), which is similar to a classical Michaelis–Menten curve for enzyme kinetics

(Krumhardt *et al*., 2013). Without cyanophage infection, the maximum phosphate uptake velocity (V_{max}) of *Prochlorococcus* NATL2A was 0.516 ± 0.155 amol phosphate cell^{-1} h^{-1} under nutrient-replete conditions and increased to 1.095 ± 0.328 amol phosphate cell^{-1} h^{-1} under P-limited conditions (Supplementary Fig. 4B), which are comparable to those of *Prochlorococcus* MED4 (Krumhardt *et al*., 2013). The increase of V_{max} under P-limited conditions is consistent with the increase of PstS protein abundance (Supplementary Fig. 2). The Michaelis–Menten constant (K_M) of *Prochlorococcus* NATL2A was 0.556 ± 0.276 μM under nutrient-replete conditions and decreased to 0.205 ± 0.086 μM under P-limited conditions (Supplementary Fig. 4C), which is within the K_M range of *Prochlorococcus* MED4 cells (0.9 ± 0.6 μM) (Krumhardt *et al*., 2013). The higher value and higher errors of *Prochlorococcus* K_M under nutrient-replete conditions were thought to be caused by the difficulty in fitting the Michaelis–Menten curve to data sets obtained using cells with low uptake rate under nutrient-replete conditions (Krumhardt *et al*., 2013).

At 6 h after infection by cyanophage P-SSM2 under P-limited conditions, V_{max} of *Prochlorococcus* NATL2A cells increased by 57% compared with the uninfected control cultures (2.05 amol phosphate cell^{-1} h^{-1}, Fig. 3A), which is consistent with the higher amount of total PstS proteins at 6 h after infection (Fig. 2F). Although the phage PstS protein has a higher K_d than that of the host PstS protein (Fig. 1B), we did not detect significant changes of K_M after cyanophage infection (Fig. 3B), probably due to the high systematic error of this measurement (Krumhardt *et al*., 2013).

At 2 h after infection, the phosphate uptake rate of infected cells did not decrease (Fig. 3A), although less PstS proteins were present (Fig. 2D), suggesting that other proteins might function to maintain the host phosphate uptake. Because *g247* and *pstS* were the only two genes in cyanophage P-SSM2 genome that were upregulated under P-limited conditions (Lin *et al*., 2016), it is plausible that gp247 might play a role in phosphate acquisition during infection. A BLASTP search using gp247 protein sequence as the query did not identify any protein of known function, but two iterations of PSI-BLAST search identified several porin proteins from *Vibrio breoganii* (*E* value ~10^{-6} and identity ~30%). To test whether gp247 can form a porin structure, we predicted its 3D model using two different servers. The AI-predicted models by tFold showed a clear transporter structure formed by beta-strands (Supplementary Fig. 5A). The structures predicted by the Phyre2 server also showed clear beta-strands structures, which could form a porin-like transporter in a homo-oligomeric organization (Supplementary Fig. 5B). In Gram-negative bacteria, porin genes have been found to be upregulated during P limitation and the expressed porins form β-barrels in the outer membrane to facilitate phosphate transport into the periplasm (Modi *et al*., 2015). The PstS protein can then binds phosphate and transports it across the periplasm membrane into the cytosol.

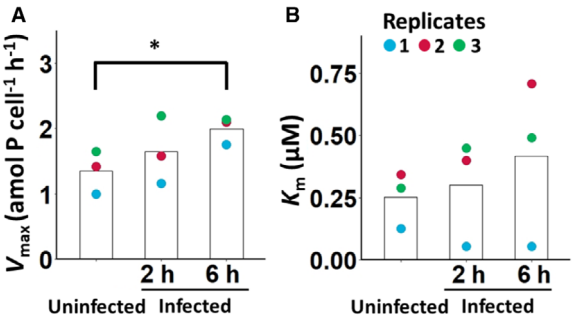

Fig. 3. Phosphate uptake of *Prochlorococcus* NATL2A cells after infection by cyanophage P-SSM2. As in Fig. 2, *Prochlorococcus* NATL2A cells were infected by cyanophage P-SSM2 at a phage/host ratio of 3 at 24 h after re-suspension in P-limited growth media. At 2 and 6 h after infection (26 and 30 h after re-suspension respectively), the maximum phosphate uptake rate (V_{max}) (A) and the Michaelis–Menten constant (K_M) (B) of the infected cells were measured. Since the phosphate uptake measurement of each culture took about 2 h, the phosphate uptake of the uninfected control cultures was measured between the 2 and 6 h infected cultures (at 28 h after re-suspension in P-limited growth media). During this period, the phosphate uptake rate of uninfected cells should remain stable, as the PstS protein abundances in the uninfected cells did not change significantly (Fig. 2D). Data points with the same colour indicate paired biological replicates conducted on the same day using the same batch of cultures. Asterisk in A indicates that V_{max} of the 6 h infected cultures is significantly larger than that of the uninfected cultures ($P = 0.015$, paired Student's *t*-test; $P = 0.048$, unpaired Student's *t*-test).

The *pstS* gene is present in 24 out of the 77 publically available cyanomyovirus genomes. We set out to further test whether a cyanophage without the *pstS* gene can enhance the host's phosphate uptake rate. We used cyanophage P-HM2, which can infect *Prochlorococcus* NATL2A but does not contain *pstS*, *phoA*, or *g247* (Sullivan *et al*., 2010). Under P-limited conditions, P-HM2 infection did not significantly affect the PstS protein abundance of *Prochlorococcus* NATL2A cells (Supplementary Fig. 6D). Consistently, P-HM2 infection did not significantly affect the host's phosphate uptake rate under both P-limited and nutrient-replete conditions (Supplementary Fig. 6E and F).

Structure of cyanophage PstS protein

Currently, several structures of PstS proteins from heterotrophic bacteria have been determined (Luecke and Quiocho, 1990; Elias *et al*., 2012), but PstS structures of cyanobacteria and cyanophages have not been solved.

To determine how PstS binds phosphate, we solved the PstS structure of cyanophage P-SSM2 at 2.25 Å resolution. To the best of our knowledge, the cyanophage PstS structure represented the first viral structure of a substrate-binding protein of an ABC transporter. The P-SSM2 PstS structure harbours a typical 'Venus flytrap' fold that is composed of two globular α/β domains held together by two β-strands (Supplementary Fig. 7A). Each α/β domain contains a central mixed five-stranded β-sheet and four or five α-helices packing against the centre (Supplementary Fig. 7A). Similar to *E. coli* PstS (Luecke and Quiocho, 1990), one phosphate molecule binds to the cleft between the two α/β domains (Supplementary Fig. 7A). Moreover, the phosphate-binding residues Ser30, Ser59, Asp77, Arg146, Asp148 and Ser150 (Supplementary Fig. 7B) are highly conserved among the PstS proteins with solved structures (Supplementary Fig. 8).

Modelling the interactions between cyanophage PstS and host PstCA

To be functional in the infected host cells, the cyanophage PstS protein needs to interact with the host PstC and PstA proteins to form a chimeric ABC transporter for phosphate uptake, since cyanophage genomes do not contain *pstC* and *pstA* genes. To investigate the interaction surface of PstS with the transmembrane PstCA complex, we tried to express and purify *Prochlorococcus* PstC and PstA proteins in *E. coli*, but could not obtain soluble proteins after multiple trials. Hence, we simulated the PstCA structure of *Prochlorococcus* NATL2A and docked P-SSM2 PstS onto the host PstCA complex (see Experimental procedures). Our simulated model showed that the phage PstS positions above the extracellular face of PstCA with its phosphate-binding pocket facing towards PstCA (Fig. 4A). PstS interacts with the host PstCA complex mainly via three interfaces, an α-helix α2 (interface 1), a η-helix η1 and flanking loops (interface 2), and a loop $L_{\alpha4-\beta7}$ (interface 3) (Fig. 4A). Detailed analysis showed that Ser61, Lys64 and Asp68 of interface 1, Lys87 of interface 2 and Thr171, Lys173 and Ala176 of interface 3 contribute to the major polar interactions with PstCA (Fig. 4B). Specifically, the interface 1 interacts with Phe163, Asn255, Asn256 and Glu278 of PstC, and the interface 2 interacts with Glu143 and Arg147 of PstC and Glu263 of PstA (Fig. 4B). In addition, the interface 3 interacts with Tyr258, Asn259 and Tyr265 of PstA (Fig. 4B). Therefore, our results suggested that the phage PstS protein can interact with the host PstCA complex to form a chimeric ABC transporter, which provides a molecular mechanism by which cyanophage infection enhances the phosphate uptake rate of cyanobacteria (Fig. 3A).

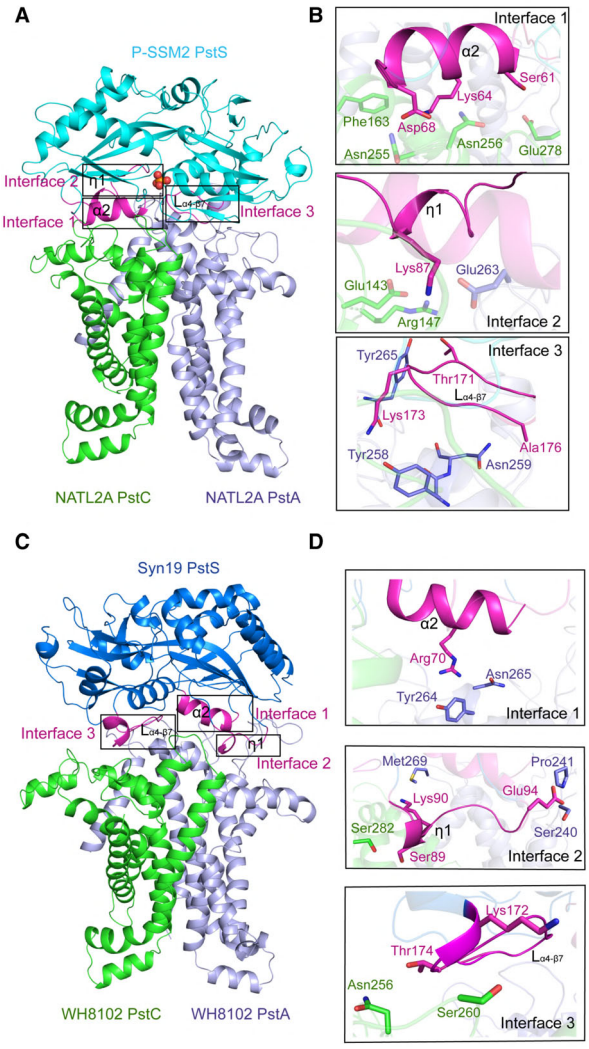

Fig. 4. Simulated models of cyanophage PstS binding to the host PstCA complex.
A. A simulated model shows the interaction of the PstS protein of cyanophage P-SSM2 (cyan) with PstC (green) and PstA (light blue) of *Prochlorococcus* NATL2A. The three interface regions of PstS that interact with the PstCA complex are shown in purple and highlighted by boxes.
B. The detailed interaction networks of the three interface regions of P-SSM2 PstS. Residues involved in the interactions are shown in sticks and are coloured in purple for PstS, green for PstC and light blue for PstA.
C. A simulated model of PstS protein of cyanophage Syn19 (blue) interacting with PstC (green) and PstA (light blue) of *Synechococcus* WH8102. Comparing to P-SSM2 PstS, the three interface regions of Syn19 PstS (purple) showed a ~180° rotation against the host PstCA complex.
D. The detailed interacting networks of the three interface regions of Syn19 PstS binding to PstCA. The colour scheme in D is the same as in B.

Two groups of cyanophage PstS proteins with different interface sequences

To investigate whether the three interface sequences are conserved in cyanophage PstS proteins, we built a

maximum-likelihood phylogenetic tree using the PstS protein sequences from the currently available cyanophage genomes, together with their host PstS sequences. Based on the tree, we grouped the PstS sequences into four groups, termed I, II, III and SphX (Fig. 5). The group I PstS contained *Prochlorococcus*, *Synechococcus* and cyanophage sequences, each forming a separate clade (Fig. 5A). PstS of cyanophage P-SSM2 is in the cyanophage clade of group I PstS sequences. The group II PstS contained cyanophage sequences and the group III PstS contained *Synechococcus* sequences (Fig. 5A). The SphX group contained *Synechococcus* sequences that are closely related to the phosphate-binding protein SphX of the freshwater cyanobacterium *Synechococcus* PCC7942 (Scanlan *et al*., 2009) (Fig. 5). Group I cyanophage PstS sequences fell into a phylogenetic clade within cyanobacterial sequences, while group II cyanophage sequences formed a distinct clade (Fig. 5A), suggesting that cyanophages might have gained the *pstS* gene from their cyanobacterial hosts in at least two separate evolutionary events.

Prochlorococcus and marine *Synechococcus* genomes all contain at least one copy of the group I *pstS* gene, and some contain additional *pstS*/*sphX* genes (Fig. 5A). For example, the genome of *Synechococcus* sp. WH8102 encodes two group I *pstS* genes, one group III *pstS* gene, and one *sphX* gene (Fig. 5A). It was hypothesized that different *pstS*/*sphX* genes may encode proteins with different phosphate-binding affinities that could be used in different environmental conditions (Scanlan *et al*., 2009). Despite multiple *pstS*/*sphX* genes, each cyanobacterial genome only encodes one *pstA* gene and one *pstC* gene (Martiny *et al*., 2006). Therefore, different PstS/SphX proteins in a cyanobacterial cell

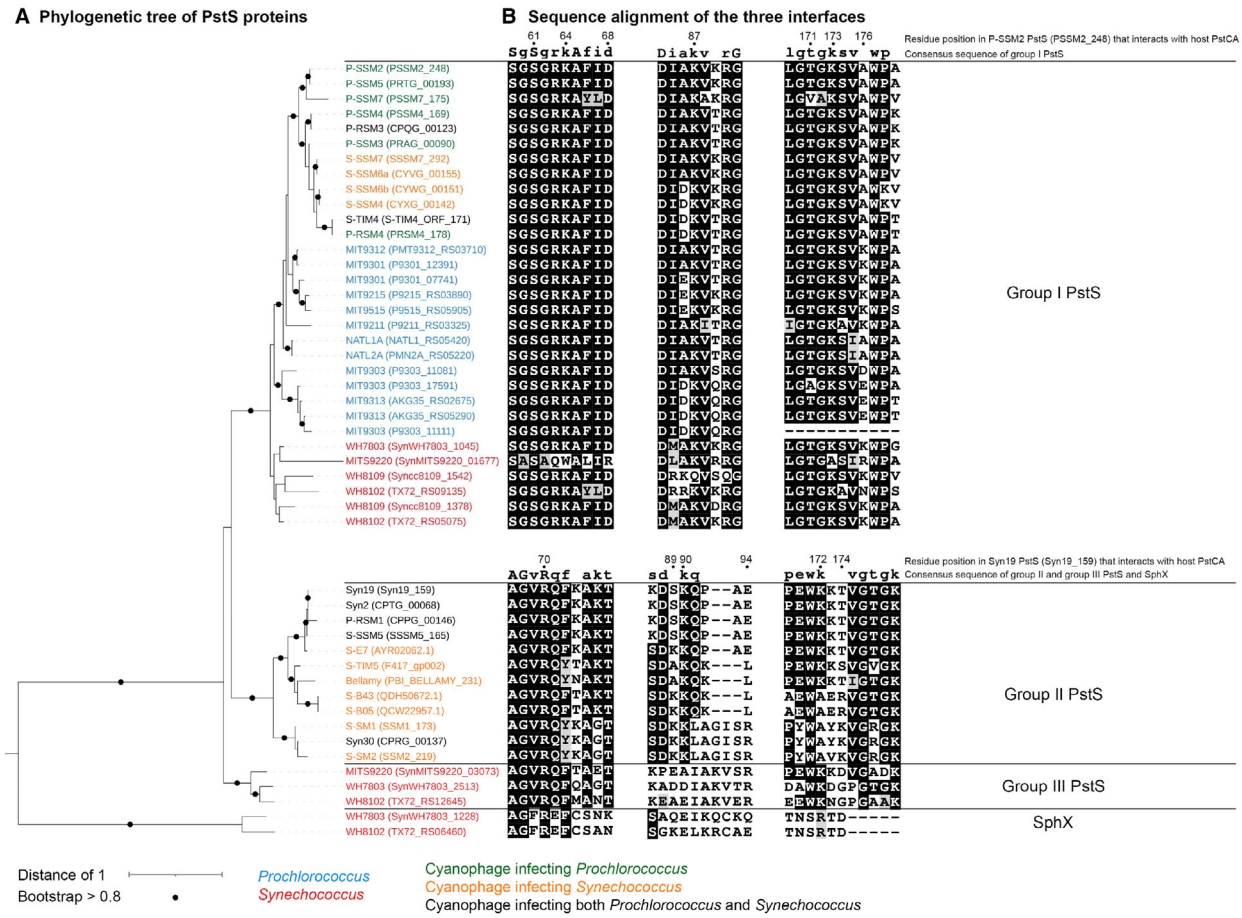

Fig. 5. Phylogeny of the PstS sequences from cyanobacteria and cyanophages.
A. Phylogenetic tree of the PstS protein sequences built using the maximum likelihood method. The PstS sequence of *Pseudomonas aeruginosa* was used as an outgroup to re-root the tree (not shown). Locus_tag or accession number of each protein is shown in parentheses. In the tree, PstS protein sequences form four groups: I, II, III and SphX.
B. Sequence alignments of the three interface regions of group I PstS proteins (top), and groups II, III and SphX proteins (bottom). The numbers above the top and bottom alignments indicate the amino acid residue positions of P-SSM2 and Syn19 PstS proteins respectively. Degree of conservation is indicated with background shading, with dark for strongly conserved and light for moderately conserved residues.

should be able to interact with the same PstCA complex. Sequence alignment showed that the three interface regions of P-SSM2 PstS are highly conserved among group I PstS sequences, but are quite different from the corresponding regions in the groups II, III and SphX sequences (Fig. 5B). Since the host PstC and PstA residues that interact with the group I PstS of cyanophage P-SSM2 are highly conserved in the sequenced *Prochlorococcus* and *Synechococcus* genomes (Supplementary Fig. 9), the group II cyanophage PstS proteins may interact with the host PstCA complex in a different way compared with the group I PstS proteins.

To explore how the group II cyanophage PstS protein interacts with the host PstCA complex, we solved the crystal structure of a group II PstS protein from cyanophage Syn19 at 1.70 Å resolution (Supplementary Fig. 10B). The P-SSM2 and Syn19 PstS proteins share a high structural similarity to each other with a root-mean-square deviation value of 0.80 Å over 255 Cα atoms (Supplementary Fig. 10D). We then simulated the PstCA structure of *Synechococcus* WH8102, which is the original host of Syn19, and docked Syn19 PstS onto the host PstCA complex (Fig. 4C). Compared with the interaction model of P-SSM2 PstS and *Prochlorococcus* NATL2A PstCA (Fig. 4A), Syn19 PstS also harbours three interfaces that are structurally similar to those of P-SSM2 PstS (Supplementary Fig. 10D). However, when the PstCA structures of *Prochlorococcus* NATL2A and *Synechococcus* WH8102 were superimposed, the Syn19 PstS shows a ∼180° rotation compared to P-SSM2 PstS (compare Fig. 4A and C). As a result, the interfaces 1 and 2 of Syn19 interact with WH8102 PstA, whereas the interface 3 binds to WH8102 PstC (Fig. 4C). On the contrary, the interfaces 1 and 2 of P-SSM2 PstS interact with NATL2A PstC, and the interface 3 binds to NATL2A PstA (Fig. 4A). The residues Arg70 of interface 1, Ser89, Lys90, Glu94 of interface 2, and Lys172 and Thr174 of interface 3 contribute to the interaction with WH8102 PstCA (Fig. 4D). Sequence alignment showed that most of the interface residues are conserved among group II cyanophage PstS proteins (Fig. 5B). Taken together, our results suggested that both group I and II cyanophage PstS proteins could recognize the host PstCA complex to organize into a functional phosphate transporter that enhances the phosphate uptake rate of infected host cells.

Discussion

In this study, we showed that the cyanophage P-SSM2 PstS protein is a functional phosphate-binding protein and is abundantly expressed during infection under P-limited conditions, resulting in more PstS proteins in the infected cultures than in the uninfected cultures. Consistently, the maximum phosphate uptake velocity of infected *Prochlorococcus* NATL2A cultures was higher than that of the uninfected cultures. In contrast, the maximum phosphate uptake velocity of *Prochlorococcus* NATL2A was not significantly affected by cyanophage P-HM2, which does not encode the *pstS* gene. The high-resolution crystal structures of cyanophage P-SSM2 PstS protein revealed key phosphate-binding residues that are conserved in bacterial and cyanophage PstS proteins. By docking the cyanophage PstS structure onto the simulated structure of the host PstCA complex, we were able to predict essential residues for the interaction of cyanophage PstS with the host PstCA complex, suggesting the formation of chimeric ABC transporters in the infected host cells. By using a combination of enzymatic, biochemical and structural analyses, our work provides molecular mechanisms by which cyanophage PstS protein is integrated into the phosphate uptake system of the cyanobacterial host cells.

The K_d value of phage PstS was significantly higher than that of the host PstS (Fig. 1B), indicating that the phage PstS has a relatively lower phosphate-binding affinity than the host PstS. Similarly, transaldolases of cyanophages have also been shown to be less efficient than those of *Prochlorococcus* hosts, which were hypothesized to be caused by shorter phage genes than the host orthologues due to phage genome size limitation (Thompson *et al*., 2011). Consistent with this hypothesis, the average lengths of cyanophage *pstS* and transaldolase genes are both shorter than the host orthologues (Thompson *et al*., 2011).

The phosphate ABC transporter is composed of PstS, the transmembrane channel proteins PstC and PstA, and the ATPase PstB (Lamarche *et al*., 2008; Hsieh and Wanner, 2010), but the currently available cyanophage genomes only contain the *pstS* gene, lacking the other three components. For ABC transporters to achieve maximal import activity, mathematic models indicate that the concentrations of substrate-binding proteins (e.g. PstS) should be higher than those of the transporters and substrates (Bosdriesz *et al*., 2015). A higher concentration of the substrate-binding protein increases the encounter rate of the transporter with the substrate and thus increases the substrate uptake rate of the transporter (Ames and Lever, 1970; Bosdriesz *et al*., 2015). Therefore, PstS protein abundance is the rate-limiting step for phosphate uptake and this may explain why cyanophages express additional PstS proteins during infection (Fig. 2E). Our previous work showed that the host *pstS* transcripts decreased by 74% at 6 h after infection under P-limited conditions and the phage *pstS* transcripts were ∼fivefold higher than the host *pstS* transcripts in the uninfected cultures (Lin *et al*., 2016). Thus, the trends of PstS protein abundances were

consistent with the transcript abundances, but with smaller changes. The variations of the transcript abundance and protein abundance of the same gene might result from translational efficiency and/or different turnover times of protein and RNA (de Sousa Abreu *et al*., 2009; Schwanhausser *et al*., 2011). With more PstS proteins, the phosphate uptake velocity of infected host cells can be enhanced (Fig. 3A), which can fulfil the high phosphorus demand of cyanophages and confer cyanophages a selective advantage under P-limited oceanic regions (Kelly *et al*., 2013; Jover *et al*., 2014).

Nutrient acquisition by infected cells affects the elemental stoichiometry of released materials after cell lysis (Jover *et al*., 2014). The dissolved organic phosphorus (DOP) released after infection comprises cellular debris and virus particles, the total amount of which depends on both the phosphorus content of uninfected host cells and the newly acquired phosphorus during infection. We showed that the maximum phosphate uptake velocity of infected *Prochlorococcus* cells increased by 57% at 6 h after infection by cyanophage P-SSM2 (Fig. 3A), indicating that more phosphate is acquired by the infected cells and thus more DOP should be released after infection. Marine virus particles have been estimated to constitute >5% of the total DOP pool in the surface waters of several oceanic regions (Jover *et al*., 2014) and cellular debris should constitute an even large proportion in the marine DOP pool. Thus, by manipulating the host phosphate ABC transporter system, cyanophages have the potential to affect phosphorus cycling in the oceans.

Acknowledgements

This study is supported by grants from the Southern Marine Science and Engineering Guangdong Laboratory (Guangzhou) (project number SMSEGL20SC01) and the Key Special Project for Introduced Talents Team of Southern Marine Science and Engineering Guangdong Laboratory (Guangzhou) (project number GML2019ZD0409). This study is supported in part by the Project of Hetao Shenzhen-Hong Kong Science and Technology Innovation Cooperation Zone (HZQB-KCZYB-2020083). We acknowledge the support of SML99147-42080013/99138-42020015. We thank Haiwei Luo for the helpful discussion and Changrui Liu for experimental assistance.

Author Contributions

Conceptualization, Q.Z.; Methodology, Q.Z., F.Z., X.L., K.C., Y.L.J., T.N. and C.-Z.Z.; Formal analysis, X.L., Y.L.J., Y.C. and F.Z.; Investigation, Q.Z., F.Z., X.L., K.C., Y.L.J., T.N., Y.C., J.F., S.D. and C.-Z.Z.; Writing – Original Draft, Q.Z., X.L., Y.L.J., F.Z.; Writing – Review and Editing, all authors.

Data Availability

PstS structures of P-SSM2 and Syn19 have been deposited in the Protein Data Bank (PDB) with the accession numbers 7XG8 and 7XG7 respectively.

References

Ames, G.F., and Lever, J. (1970) Components of histidine transport: histidine-binding proteins and hisP protein. *Proc Natl Acad Sci U S A* **66**: 1096–1103.

Bosdriesz, E., Magnusdottir, S., Bruggeman, F.J., Teusink, B., and Molenaar, D. (2015) Binding proteins enhance specific uptake rate by increasing the substrate-transporter encounter rate. *FEBS J* **282**: 2394–2407.

Brautigam, C.A., Ouyang, Z., Deka, R.K., and Norgard, M.V. (2014) Sequence, biophysical, and structural analyses of the PstS lipoprotein (BB0215) from *Borrelia burgdorferi* reveal a likely binding component of an ABC-type phosphate transporter. *Protein Sci* **23**: 200–212.

Chen, V.B., Arendall, W.B., 3rd, Headd, J.J., Keedy, D.A., Immormino, R.M., Kapral, G.J., *et al*. (2010) MolProbity: all-atom structure validation for macromolecular crystallography. *Acta Crystallogr D Biol Crystallogr* **66**: 12–21.

Coleman, M.L., and Chisholm, S.W. (2010) Ecosystem-specific selection pressures revealed through comparative population genomics. *Proc Natl Acad Sci U S A* **107**: 18634–18639.

Collaborative Computational Project, Number 4. (1994) The CCP4 suite: programs for protein crystallography. *Acta Crystallogr D Biol Crystallogr* **50**: 760–763.

Cox, A.D., and Saito, M.A. (2013) Proteomic responses of oceanic *Synechococcus* WH8102 to phosphate and zinc scarcity and cadmium additions. *Front Microbiol* **4**: 387.

de Sousa Abreu, R., Penalva, L.O., Marcotte, E.M., and Vogel, C. (2009) Global signatures of protein and mRNA expression levels. *Mol Biosyst* **5**: 1512–1526.

Elias, M., Wellner, A., Goldin-Azulay, K., Chabriere, E., Vorholt, J.A., Erb, T.J., and Tawfik, D.S. (2012) The molecular basis of phosphate discrimination in arsenate-rich environments. *Nature* **491**: 134–137.

Emsley, P., and Cowtan, K. (2004) Coot: model-building tools for molecular graphics. *Acta Crystallogr D Biol Crystallogr* **60**: 2126–2132.

Enav, H., Kirzner, S., Lindell, D., Mandel-Gutfreund, Y., and Beja, O. (2018) Adaptation to sub-optimal hosts is a driver of viral diversification in the ocean. *Nat Commun* **9**: 4698.

Feingersch, R., Philosof, A., Mejuch, T., Glaser, F., Alalouf, O., Shoham, Y., and Beja, O. (2012) Potential for phosphite and phosphonate utilization by Prochlorococcus. *ISME J* **6**: 827–834.

Fu, F.X., Zhang, Y.H., Bell, P.R.F., and Hutchins, D.A. (2005) Phosphate uptake and growth kinetics of Trichodesmium (Cyanobacteria) isolates from the North Atlantic Ocean and the Great Barrier Reef, Australia. *J Phycol* **41**: 62–73.

Fuszard, M.A., Wright, P.C., and Biggs, C.A. (2010) Cellular acclimation strategies of a minimal picocyanobacterium to phosphate stress. *FEMS Microbiol Lett* **306**: 127–134.

Hsieh, Y.J., and Wanner, B.L. (2010) Global regulation by the seven-component Pi signaling system. *Curr Opin Microbiol* **13**: 198–203.

Hua, J., Huet, A., Lopez, C.A., Toropova, K., Pope, W.H., Duda, R.L., *et al*. (2017) Capsids and genomes of jumbo-sized bacteriophages reveal the evolutionary reach of the HK97 fold. *mBio* **8**: e01579-17.

Jiang, T., Guo, C., Wang, M., Wang, M., You, S., Liu, Y., *et al*. (2020) Isolation and complete genome sequence of a novel cyanophage, S-B05, infecting an estuarine Synechococcus strain: insights into environmental adaptation. *Arch Virol* **165**: 1397–1407.

Jover, L.F., Effler, T.C., Buchan, A., Wilhelm, S.W., and Weitz, J.S. (2014) The elemental composition of virus particles: implications for marine biogeochemical cycles. *Nat Rev Microbiol* **12**: 519–528.

Kamennaya, N.A., Geraki, K., Scanlan, D.J., and Zubkov, M. V. (2020) Accumulation of ambient phosphate into the periplasm of marine bacteria is proton motive force dependent. *Nat Commun* **11**: 2642.

Karl, D.M. (2014) Microbially mediated transformations of phosphorus in the sea: new views of an old cycle. *Ann Rev Mar Sci* **6**: 279–337.

Kelly, L., Ding, H., Huang, K.H., Osburne, M.S., and Chisholm, S.W. (2013) Genetic diversity in cultured and wild marine cyanomyoviruses reveals phosphorus stress as a strong selective agent. *ISME J* **7**: 1827–1841.

Krumhardt, K.M., Callnan, K., Roache-Johnson, K., Swett, T., Robinson, D., Reistetter, E.N., *et al*. (2013) Effects of phosphorus starvation versus limitation on the marine cyanobacterium *Prochlorococcus* MED4 I: uptake physiology. *Environ Microbiol* **15**: 2114–2128.

Lamarche, M.G., Wanner, B.L., Crepin, S., and Harel, J. (2008) The phosphate regulon and bacterial virulence: a regulatory network connecting phosphate homeostasis and pathogenesis. *FEMS Microbiol Rev* **32**: 461–473.

Letunic, I., and Bork, P. (2016) Interactive tree of life (iTOL) v3: an online tool for the display and annotation of phylogenetic and other trees. *Nucleic Acids Res* **44**: W242–W245.

Lin, X., Ding, H., and Zeng, Q. (2016) Transcriptomic response during phage infection of a marine cyanobacterium under phosphorus-limited conditions. *Environ Microbiol* **18**: 450–460.

Lomas, M.W., Bonachela, J.A., Levin, S.A., and Martiny, A. C. (2014) Impact of ocean phytoplankton diversity on phosphate uptake. *Proc Natl Acad Sci U S A* **111**: 17540–17545.

Luecke, H., and Quiocho, F.A. (1990) High specificity of a phosphate transport protein determined by hydrogen bonds. *Nature* **347**: 402–406.

Madeira, F., Park, Y.M., Lee, J., Buso, N., Gur, T., Madhusoodanan, N., *et al*. (2019) The EMBL-EBI search and sequence analysis tools APIs in 2019. *Nucleic Acids Res* **47**: W636–W641.

Martinez, A., Osburne, M.S., Sharma, A.K., DeLong, E.F., and Chisholm, S.W. (2012) Phosphite utilization by the marine picocyanobacterium *Prochlorococcus* MIT9301. *Environ Microbiol* **14**: 1363–1377.

Martiny, A.C., Coleman, M.L., and Chisholm, S.W. (2006) Phosphate acquisition genes in *Prochlorococcus* ecotypes: evidence for genome-wide adaptation. *Proc Natl Acad Sci U S A* **103**: 12552–12557.

Martiny, A.C., Huang, Y., and Li, W. (2009) Occurrence of phosphate acquisition genes in *Prochlorococcus* cells from different ocean regions. *Environ Microbiol* **11**: 1340–1347.

Medveczky, N., and Rosenberg, H. (1970) The phosphate-binding protein of *Escherichia coli*. *Biochim Biophys Acta (BBA) - Biomembranes* **211**: 158–168.

Michaelis, L., Menten, M.L., Johnson, K.A., and Goody, R.S. (2011) The original Michaelis constant: translation of the 1913 Michaelis-Menten paper. *Biochemistry* **50**: 8264–8269.

Modi, N., Ganguly, S., Barcena-Uribarri, I., Benz, R., van den Berg, B., and Kleinekathofer, U. (2015) Structure, dynamics, and substrate specificity of the OprO porin from *Pseudomonas aeruginosa*. *Biophys J* **109**: 1429–1438.

Moore, L.R., Ostrowski, M., Scanlan, D.J., Feren, K., and Sweetsir, T. (2005) Ecotypic variation in phosphorus-acquisition mechanisms within marine picocyanobacteria. *Aquat Microb Ecol* **39**: 257–269.

Moore, L.R., Post, A.F., Rocap, G., and Chisholm, S.W. (2002) Utilization of different nitrogen sources by the marine cyanobacteria Prochlorococcus and Synechococcus. *Limnol Oceanogr* **47**: 989–996.

Nagaya, M., Aiba, H., and Mizuno, T. (1994) The *sphR* product, a two-component system response regulator protein, regulates phosphate assimilation in *Synechococcus* sp. strain PCC 7942 by binding to two sites upstream from the *phoA* promoter. *J Bacteriol* **176**: 2210–2215.

Oldham, M.L., Khare, D., Quiocho, F.A., Davidson, A.L., and Chen, J. (2007) Crystal structure of a catalytic intermediate of the maltose transporter. *Nature* **450**: 515–521.

Ostrowski, M., Mazard, S., Tetu, S.G., Phillippy, K., Johnson, A., Palenik, B., *et al*. (2010) PtrA is required for coordinate regulation of gene expression during phosphate stress in a marine *Synechococcus*. *ISME J* **4**: 908–921.

Otwinowski, Z., and Minor, W. (1997) Processing of X-ray diffraction data collected in oscillation mode. *Methods Enzymol* **276**: 307–326.

Partensky, F., Hess, W.R., and Vaulot, D. (1999) *Prochlorococcus*, a marine photosynthetic prokaryote of global significance. *Microbiol Mol Biol Rev* **63**: 106–127.

Poole, K., and Hancock, R.E. (1984) Phosphate transport in *Pseudomonas aeruginosa*. Involvement of a periplasmic phosphate-binding protein. *Eur J Biochem* **144**: 607–612.

Reistetter, E.N., Krumhardt, K., Callnan, K., Roache-Johnson, K., Saunders, J.K., Moore, L.R., and Rocap, G. (2013) Effects of phosphorus starvation versus limitation on the marine cyanobacterium *Prochlorococcus* MED4 II: gene expression. *Environ Microbiol* **15**: 2129–2143.

Sabehi, G., Shaulov, L., Silver, D.H., Yanai, I., Harel, A., and Lindell, D. (2012) A novel lineage of myoviruses infecting cyanobacteria is widespread in the oceans. *Proc Natl Acad Sci U S A* **109**: 2037–2042.

Scanlan, D.J., Mann, N.H., and Carr, N.G. (1993) The response of the picoplanktonic marine cyanobacterium *Synechococcus* species WH7803 to phosphate starvation involves a protein homologous to the periplasmic

phosphate-binding protein of *Escherichia coli*. *Mol Microbiol* **10**: 181–191.
Scanlan, D.J., Ostrowski, M., Mazard, S., Dufresne, A., Garczarek, L., Hess, W.R., *et al*. (2009) Ecological genomics of marine picocyanobacteria. *Microbiol Mol Biol Rev* **73**: 249–299.
Schwanhausser, B., Busse, D., Li, N., Dittmar, G., Schuchhardt, J., Wolf, J., *et al*. (2011) Global quantification of mammalian gene expression control. *Nature* **473**: 337–342.
Stamatakis, A. (2014) RAxML version 8: a tool for phylogenetic analysis and post-analysis of large phylogenies. *Bioinformatics* **30**: 1312–1313.
Sullivan, M.B., Coleman, M.L., Weigele, P., Rohwer, F., and Chisholm, S.W. (2005) Three *Prochlorococcus* cyanophage genomes: signature features and ecological interpretations. *PLoS Biol* **3**: e144.
Sullivan, M.B., Huang, K.H., Ignacio-Espinoza, J.C., Berlin, A.M., Kelly, L., Weigele, P.R., *et al*. (2010) Genomic analysis of oceanic cyanobacterial myoviruses compared with T4-like myoviruses from diverse hosts and environments. *Environ Microbiol* **12**: 3035–3056.
Sullivan, M.B., Waterbury, J.B., and Chisholm, S.W. (2003) Cyanophages infecting the oceanic cyanobacterium *Prochlorococcus*. *Nature* **424**: 1047–1051.
Suzuki, S., Ferjani, A., Suzuki, I., and Murata, N. (2004) The SphS-SphR two component system is the exclusive sensor for the induction of gene expression in response to phosphate limitation in *Synechocystis*. *J Biol Chem* **279**: 13234–13240.
Tetu, S.G., Brahamsha, B., Johnson, D.A., Tai, V., Phillippy, K., Palenik, B., and Paulsen, I.T. (2009) Microarray analysis of phosphate regulation in the marine cyanobacterium *Synechococcus* sp. WH8102. *ISME J* **3**: 835–849.
Thingstad, T.F., Krom, M.D., Mantoura, R.F., Flaten, G.A., Groom, S., Herut, B., *et al*. (2005) Nature of phosphorus limitation in the ultraoligotrophic eastern Mediterranean. *Science* **309**: 1068–1071.
Thompson, L.R., Zeng, Q., Kelly, L., Huang, K.H., Singer, A. U., Stubbe, J., and Chisholm, S.W. (2011) Phage auxiliary metabolic genes and the redirection of cyanobacterial host carbon metabolism. *Proc Natl Acad Sci U S A* **108**: E757–E764.
Van Mooy, B.A., Fredricks, H.F., Pedler, B.E., Dyhrman, S. T., Karl, D.M., Koblizek, M., *et al*. (2009) Phytoplankton in the ocean use non-phosphorus lipids in response to phosphorus scarcity. *Nature* **458**: 69–72.
Van Mooy, B.A., Rocap, G., Fredricks, H.F., Evans, C.T., and Devol, A.H. (2006) Sulfolipids dramatically decrease phosphorus demand by picocyanobacteria in oligotrophic marine environments. *Proc Natl Acad Sci U S A* **103**: 8607–8612.
Viaene, L., Annaert, P., de Loor, H., Poesen, R., Evenepoel, P., and Meijers, B. (2013) Albumin is the main plasma binding protein for indoxyl sulfate and p-cresyl sulfate. *Biopharm Drug Dispos* **34**: 165–175.
Wang, M., Gao, C., Jiang, T., You, S., Jiang, Y., Guo, C., *et al*. (2020) Genomic analysis of Synechococcus phage S-B43 and its adaption to the coastal environment. *Virus Res* **289**: 198155.
Wang, Z., Luecke, H., Yao, N., and Quiocho, F.A. (1997) A low energy short hydrogen bond in very high resolution structures of protein receptor–phosphate complexes. *Nat Struct Biol* **4**: 519–522.
Wu, J., Sunda, W., Boyle, E.A., and Karl, D.M. (2000) Phosphate depletion in the western North Atlantic Ocean. *Science* **289**: 759–762.
Zborowsky, S., and Lindell, D. (2019) Resistance in marine cyanobacteria differs against specialist and generalist cyanophages. *Proc Natl Acad Sci U S A* **116**: 16899–16908.
Zeng, Q., and Chisholm, S.W. (2012) Marine viruses exploit their host's two-component regulatory system in response to resource limitation. *Curr Biol* **22**: 124–128.
Zubkov, M.V., Martin, A.P., Hartmann, M., Grob, C., and Scanlan, D.J. (2015) Dominant oceanic bacteria secure phosphate using a large extracellular buffer. *Nat Commun* **6**: 7878.

Supporting Information

Additional Supporting Information may be found in the online version of this article at the publisher's web-site:

Fig. 1. Specificity of antibodies against the PstS proteins of *Prochlorococcus* NATL2A and cyanophage P-SSM2. The His-tagged recombinant PstS proteins of *Prochlorococcus* NATL2A and cyanophage PSSM2 were purified and separated on 12% SDS-PAGE. Proteins were stained with Coomassie Blue (A) or transferred to membranes and probed using antibodies against NATL2A PstS (B) and P-SSM2 PstS (C). In B and C, 0.5 μg protein was loaded in each lane. Protein sizes are shown on the left of each gel.

Fig. 2. PstS protein abundances of *Prochlorococcus* NATL2A under nutrient-replete and P-limited conditions. A. SDS-PAGE. *Prochlorococcus* NATL2A cells were spun down and re-suspended in nutrient replete or P-limited media. Cultures were collected at different time points after re-suspension. Total protein from 108 cells was loaded in each lane and separated in SDS-PAGE. The time after re-suspension is shown above each lane. Protein sizes are shown on the left of the gel. The arrow indicates the PstS protein band (~34 kDa). B. Western blot. Proteins from replicate SDS-PAGE were transferred to a membrane and probed with the antibody against NATL2A PstS.

Fig. 3. Quantification of PstS proteins in *Prochlorococcus* NATL2A cells using quantitative western blotting. A. A representative standard curve generated using the signal volumes of protein bands in the quantitative western blots shown in Figure 2C (top panel). B. Based on the standard curve, amounts of PstS proteins per cell were calculated.

Fig. 4. Phosphate uptake of uninfected *Prochlorococcus* NATL2A cells. *Prochlorococcus* NATL2A cells were spun down and re-suspended in nutrient-replete or P-limited growth media. At 28 h after re-suspension, phosphate uptake velocity of uninfected *Prochlorococcus* NATL2A cells was measured as a function of cold phosphate. A shows representative phosphate uptake curves of cells under nutrient-replete and P-limited conditions. Dashed lines in A represent the best fit of a hyperbolic curve. Using the phosphate uptake curves, the maximum uptake velocity (V_{max})

(B) and the Michaelis–Menten constant (K_M) (C) of *Prochlorococcus* NATL2A were calculated. Asterisks in B and C indicate significant differences ($P < 0.05$, Student's *t*-test).

Fig. 5. Predicted structures of cyanophage P-SSM2 gp247. Structure of cyanophage gp247 was predicted using two methods. A. De novo folding structure was predicted by the tFold server (https://drug.ai.tencent.com/console/en/tfold). The structure with the highest ranking is shown. B. Structure of gp247 was predicted by the template-based modelling method via Phyre2 (http://www.sbg.bio.ic.ac.uk/phyre2) based on the three-dimensional structure of the outer membrane porin OprF of *Pseudomonas aeruginosa* (Phyre2 fold library ID: c4rlca; confidence score: 91.3).

Fig. 6. PstS protein abundance and phosphate uptake of *Prochlorococcus* NATL2A cells after infection by cyanophage P-HM2. A. *Prochlorococcus* NATL2A cells were spun down and re-suspended in nutrient-replete or P-limited growth media. B. At 24 h after re-suspension, cells were infected by cyanophage P-HM2 at a phage/host ratio of 3. Extracellular phages were measured by quantitative PCR using primers for the phage *DNApol* gene. Error bars in A and B indicate standard deviations from three biological replicates. C. Similar to Figure 2C, quantitative western blots were conducted to quantify host PstS protein abundances at 2 h and 6 h after infection under P-limited conditions, with five biological replicates (R1 to R5). D. Using the blots in C, host PstS abundances in uninfected and infected cells under P-limited conditions were compared and there was no significant difference. At 6 h after infection (30 h after re-suspension), the maximum uptake velocity (V_{max}) (E) and the Michaelis–Menten constant (*K*M) (F) of infected *Prochlorococcus* NATL2A were measured under both nutrient-replete and P-limited conditions. V_{max} and K_M of uninfected cultures were measured at 28 h after re-suspension to allow enough time to complete the measurement of each culture. Data points with the same symbol in E and F indicate paired biological replicates conducted in the same day using the same batch of cultures. For both V_{max} and K_M values, there was no significant difference between uninfected and infected cultures under the same nutrient condition.

Fig. 7. Overall structure of P-SSM2 PstS in complex with PO4. A. Cartoon representation of the overall structure of the P-SSM2 PstS protein in complex with a PO4 molecule (shown in red). Secondary structural elements of PstS are labelled sequentially. B. Detailed view of the PO4-binding site, with PO4-interacting residues shown as sticks.

Fig. 8. Sequence alignment of PstS proteins. The secondary structural elements of P-SSM2 PstS are shown at the top of the PstS sequence alignment. The numbers above the sequence alignment indicate the residue numbers of P-SSM2 PstS. The phosphate-interacting residues of P-SSM2 PstS are marked by red stars. Among these residues, Ser59, Asp77, Arg146, Asp148, and Ser150 are conserved in all the PstS proteins listed here. Ser30 is conserved in cyanophage and cyanobacterial proteins, and is replaced by a chemically similar amino acid threonine in other PstS proteins.

Fig. 9. Sequence alignment of cyanobacterial PstC and PstA proteins. Protein sequence alignments are shown for cyanobacterial PstC (A) and PstA (B). The background shading indicates the degree of conservation, with black for strongly conserved and grey for moderately conserved residues. Putative residues interacting with group I PstS are marked with blue circles and those interacting with group II PstS are marked with red triangles.

Fig. 10. Overall structures of PstS proteins. A. The PstS structure of cyanophage P-SSM2 in complex with PO4 (red symbol). B. The PstS structure of cyanophage Syn19 in complex with PO4. C. A model of PstS structure of *Prochlorococcus* NATL2A in complex with PO4. D. Superposition of PstS proteins of P-SSM2 (cyan), Syn19 (blue) and NATL2A (light pink). The segments involved in interaction with PstCA are highlighted.

Fig. 11. Phosphate uptake by *Prochlorococcus* NATL2A over time. Axenic *Prochlorococcus* NATL2A cells were grown under P-limited (left panel) or P-replete (right panel) conditions. To measure phosphate uptake rates, *Prochlorococcus* cells were pelleted by centrifugation and re-suspended with the Pro99 medium without addition of phosphate. Re-suspended cells were amended with 10 μM cold NaH_2PO_4 and trace amount of 32P-labelled orthophosphoric acid (~1 μCi, Perkin Elmer). Every 30 min, 1 ml culture was filtered through a 0.22 μm polycarbonate filter that was supported by a Whatman GF/F filter. During filtration, the vacuum pressure was ~100 mm Hg. The phosphate uptake amount by 1 ml culture was estimated by measuring the radioactivity on each filter.

Table 1. PCR primers.

Table 2. Parameters of P-SSM2 PstS structure.

Table 3. Parameters of Syn19 PstS structure.